

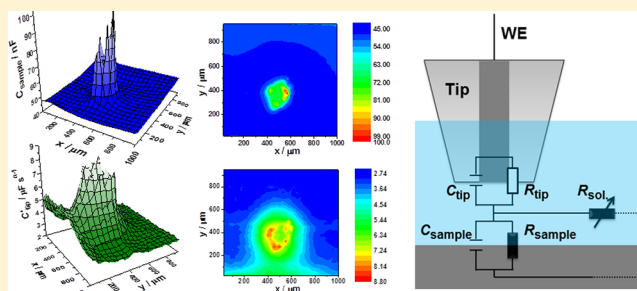
Localized Electrochemical Impedance Spectroscopy: Visualization of Spatial Distributions of the Key Parameters Describing Solid/Liquid Interfaces

Aliaksandr S. Bandarenka,^{*,†} Kathrin Eckhard,[‡] Artjom Maljusch,[‡] and Wolfgang Schuhmann^{*,‡}

[†]Center for Electrochemical Sciences - CES, Ruhr-Universität Bochum, Universitätsstrasse 150, D-44780 Bochum, Germany

[‡]Analytische Chemie - Elektroanalytik & Sensorik, Ruhr-Universität Bochum, Universitätsstrasse 150, D-44780 Bochum, Germany

ABSTRACT: Acquisition of localized electrochemical impedance spectra as a function of spatial coordinates combined with novel approaches of data analysis brings a key for visualization of two-dimensional distributions of important parameters describing solid/liquid interfaces. They include the capacitance of the electric double layer, the resistance of the interfacial charge transfer, capacitances of adsorption, or other parameters depending on the properties of the system. Additionally, the proposed approach eliminates many common methodological problems of localized electrochemical impedance microscopies related to the frequency dependence of the actual pictures and difficulties with raw data interpretation. Thus, it offers a unique insight into the localized processes at the interface which is not possible to achieve using classical techniques.



Monitoring and understanding the processes which occur at the interface between liquid electrolytes and solids are of increasing importance in many fields of modern science and technology.^{1–8} This is particularly vital in the case of nonhomogeneous samples, for example in corrosion science, in order to be able to detect local generation of corrosion sites and to elucidate mechanisms of degradation of protective films.^{9,10} The development of functional coatings and catalyst layers which are designed to operate in contact with liquids also requires versatile tools for their *in situ* characterization capable of providing the necessary information with adequate spatial resolution, e.g. in the micrometer range. Other areas of application include biochemistry, biology, medical applications, electrocatalysis, etc.

Characterization of the interfaces between solids and liquids with various spatial resolutions, however, represents a significant challenge. While common scanning probe techniques, such as atomic force microscopy or scanning tunneling microscopy mainly provide the information about different properties of the surface,^{11,12} only a few techniques are able to give valuable information about the properties of the interface itself, as a function of spatial coordinates. One of these few techniques is the localized electrochemical impedance spectroscopy (LEIS)^{13–17} and its more advanced variations, for example alternating current scanning electrochemical microscopy (AC-SECM).^{18–21}

LEIS and AC-SECM allow identification and visualization of microscopic domains with different interfacial properties and with different electrochemical activities toward reactions which occur in contact with electrolytes.^{9,10} These methods are very robust and can be used for imaging the surfaces of significantly

different properties, in solutions of low conductivity, either in the absence or in the presence of redox mediators. As an output, localized impedance measurements generate a series of surface images describing the *ac*-response (modulus of impedance, phase shift, imaginary and real parts of the impedance) as a function of the probe position. Normally, only one single frequency is used for this purpose. However, several other approaches have been developed to advance the methodology. For example, frequency-dependent alternating-current scanning electrochemical microscopy (4D AC-SECM)¹⁰ can visualize the surface at different frequencies of the *ac*-probing signals as a result of a single experiment. This provides flexibility to choose the best visualization in each particular case.

While state-of-the-art LEIS techniques are able to optimize acquisition of impedance data as a function of the probe position at different frequencies, the physicochemical and analytical interpretation of these data is not always straightforward. It often turns out that the exact LEIS-picture depends on the selection of the *ac*-frequency. This effect originates from the fact that different processes taking place simultaneously at the surface of the sample and at the microscope tip can have dissimilar time constants and, therefore, contribute differently at different frequencies to the overall measured response. This restricts the application of these techniques, as it is often problematic to predict the frequency range where the contribution of the processes of interest is maximal and

Received: December 2, 2012

Accepted: January 20, 2013

Published: January 20, 2013

where the contribution of e.g. the interfering response of the tip is minimal.

In this work, we demonstrate how the advantage of the multifrequency response acquisition (available in 4D AC-SECM)^{9,10} being combined with recent achievements in the analysis of large impedance data sets^{22–24} can considerably increase the informative power of LEIS techniques. Fitting the frequency dependent impedance data at each x,y -point (localized impedance spectra) to physical models describing the measurement system and the sample can resolve the contributions from the processes with different time constants. Consequently, this gives the dependencies of many important parameters (for instance, the charge transfer resistance or the double layer capacitance at the sample surface) on spatial coordinates. Additionally, the contributions originating from the scanning microelectrode tip can be either eliminated or taken into account depending on analytical purposes. This can provide a unique insight into the localized processes at the sample/electrolyte interface which is not possible to achieve using classical LEIS techniques. The proposed approach is demonstrated using a model sample with a local defect made in a thin protective organic coating covering a metallic surface.

EXPERIMENTAL SECTION

4D AC-SECM data acquisition procedure is described in detail elsewhere.^{9,10} Briefly, automatic recording of full-frequency impedance spectra at each point during the scans was performed in the frequency range from 8 kHz to 270 Hz. In total 1520 impedance spectra were recorded, and each spectrum consists of 20 frequency points. Lower frequencies were avoided as a compromise between the amount of necessary information to be extracted from the spectra by the fitting and reasonable experimental time for the data acquisition. The quality of the localized impedance spectra was tested with “linear” and “logarithmic” Kramers–Kronig check procedures. The quality of the fitting was controlled by the root-mean-square deviations and estimated individual parameter errors, similar to ref 25. The former were compared with those obtained by the Kramers–Kronig check procedures to ensure the validity of the model and the correctness of the fitting. The following parameters and conditions were used for the x,y -scans: diameter of the glass coated Pt-microelectrode tip $d_{\text{Pt-tip}} = 25 \mu\text{m}$, 1 mM KClO_4 electrolyte, probing signal amplitude $V_{\text{pp}} = 100 \text{ mV}$, scan area $S = 1000 \mu\text{m} \times 1000 \mu\text{m}$. It should be noted that the selection of the probing signal amplitude depends on the properties of the system under investigation. The relatively high amplitude used in this work was the maximum allowed by the Kramers–Kronig check procedures (i.e., by system properties), where the electrochemical system behaved quasi-linearly under the *ac*-probing.

Low-carbon steel coated with tin and subsequently covered with a 9–15 μm layer of epoxyphenolic varnish was used as the model sample. The insulating polymer layer had been damaged prior to the experiment in order to expose the underlying metal. A circular defect of approximately 220 μm in diameter had been introduced by punching the polymer coating with a needle.

The large experimental impedance data set generated by 4D AC-SECM was analyzed (using homemade “EIS Data Analysis v.02” software) according to the procedure described in detail elsewhere.²² Briefly, the fitting procedure uses the idea of successive Bayesian estimation²⁶ where estimation of the parameters of the EIS-models is performed successively, from

one impedance spectrum to another, using the complex nonlinear least-squares (CNLS) method. The results obtained on the previous step are used as *a priori* values (in the Bayesian form) for the analysis of the next spectrum. Efficient hybrid fitting algorithm described in ref 22 is used to provide high stability of the sequential CNLS fitting, allowing semiautomatic data analysis on a reasonable time scale (1520 spectra were fitted within 16 min 30 s using a desktop computer with a 3 GHz processor, 4GB RAM; so the fitting required comparable or significantly less time than the data acquisition).

RESULTS AND DISCUSSION

Figure 1A shows the 4D AC-SECM measurements scheme together with a detailed equivalent electric circuit (EEC)

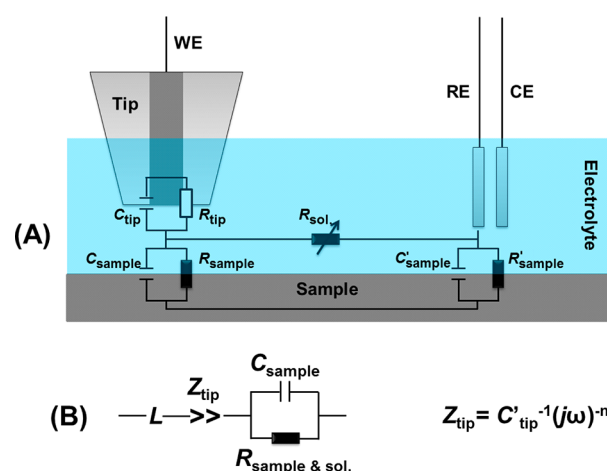


Figure 1. (A) Schematic representation of the localized impedance experiments with a detailed equivalent electric circuit describing the measured response. (B) A simplified equivalent circuit describing the contributions of the sample (C_{sample} , R_{sample}) and the tip (Z_{tip}) responses; an additional inductance is necessary to account for the effects of the potentiostat at higher frequencies. WE, RE, and CE denote the working, reference, and counter electrodes, respectively.

describing the overall measured response. In the detailed EEC (Figure 1A), R_{sol} is the solution resistance, which changes with the absolute distance between the microelectrode tip and the sample surface as well as with the distance between the reference and working (tip) electrodes. R_{tip} and C_{tip} are the resistance and capacitance which are related to the tip, respectively. Further, knowing the properties of the sample used in this work and the frequency range, it is possible to describe the electrode/electrolyte interface with just a parallel combination of the charge transfer resistance R'_{sample} and the double layer (or interfacial) capacitance C'_{sample} , with the particular case for the R_{sample} and C_{sample} at the specific area that is covered by the glass shield of the tip.^{9,10} The latter parameters will change if the local interface (and/or surface) properties would change and, therefore, would contain valuable analytical information. The EEC shown in Figure 1A reflects the situation that when the tip (working electrode) is in close proximity to the sample surface, the current can either flow through the solution or via the sample and corresponding sample/electrolyte interfaces.

For the fitting of the local impedance spectra to the model, the latter needs to be simplified taking into account several basic assumptions. The first assumption is that the charge transfer resistance at the tip R_{tip} is very high, as the electrolyte

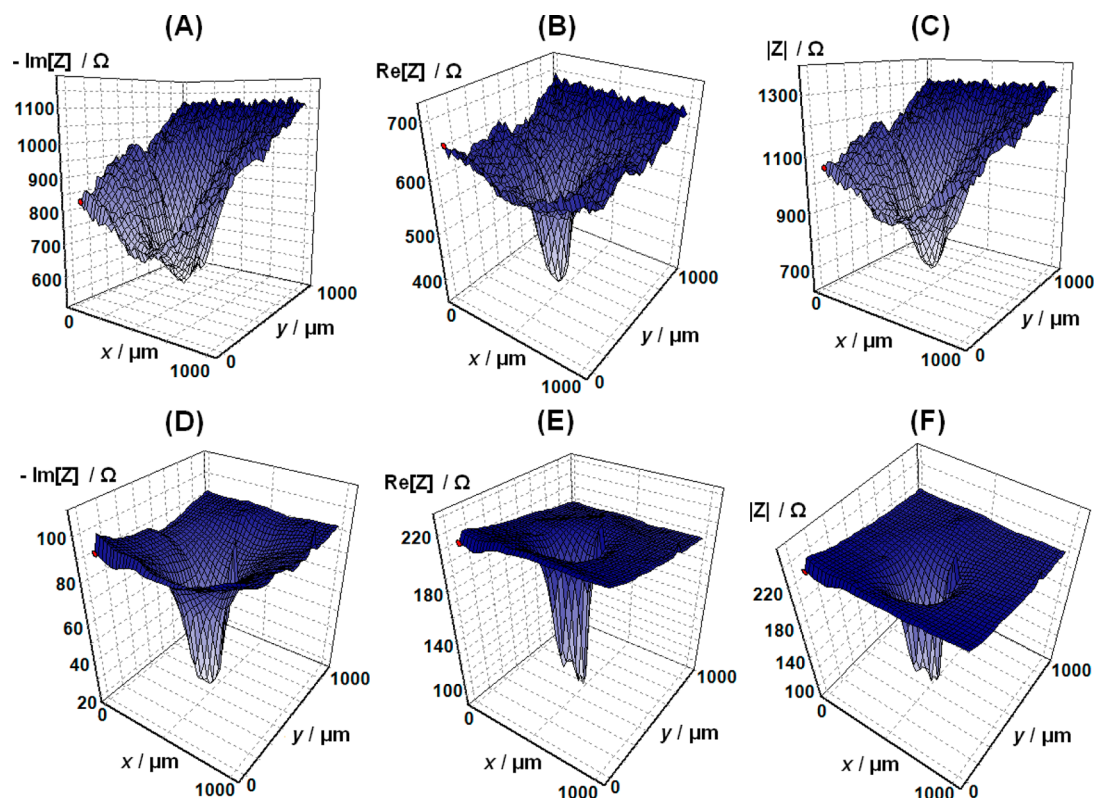


Figure 2. Examples of the dependencies of (A,D) imaginary parts, (B,E) real parts, and (C,F) the absolute values of the impedance on spatial coordinates (x and y) at (A-C) 270 Hz and (D-F) 8 kHz; the surface imaging is dependent on the probing frequency.

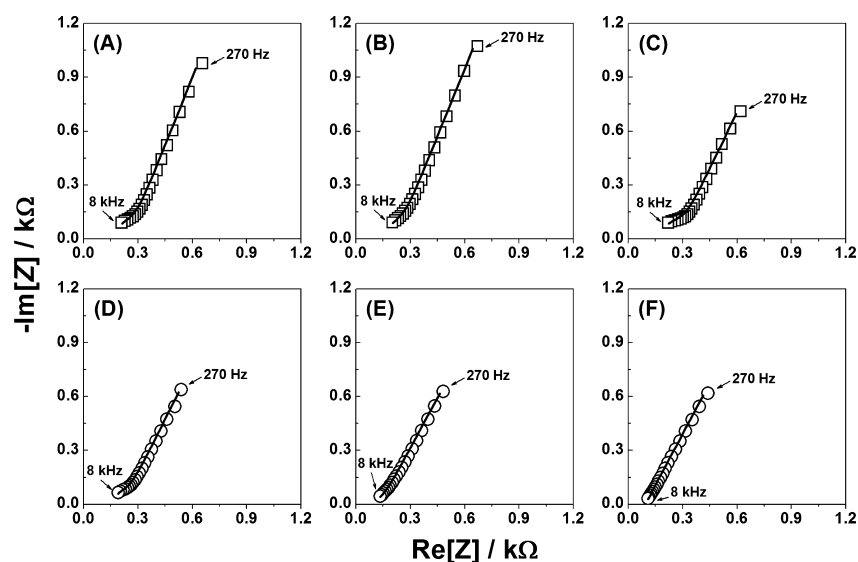


Figure 3. Examples of the typical localized impedance spectra (open symbols) taken (A-C) at the surface coated with a nonconducting polymer and (D-F) over the artificially created defect exposing the underlying metal surface to the 1 mM KClO_4 electrolyte. Solid lines represent the fitting to the equivalent circuit shown in Figure 1B.

does not contain electrochemically active species capable of influencing significantly the measurements at the selected potentials. Therefore, the response of the tip is expected to be predominantly capacitive, due to the response of the double layer formed at the tip/electrolyte interface (with an influence of some parasitic capacitance of the microelectrode itself). The so-called constant phase element (CPE) normally describes the response of this kind of interfaces, accounting for a nonideal capacitive behavior of solid metal electrodes in contact with

electrolytes^{27–30} with the following equation for the impedance $Z_{\text{CPE,tip}} = C'_{\text{tip}}{}^{-1}(j\omega)^{-n}$ (where C'_{tip} is proportional to the double layer capacitance related to the tip, j is the imaginary unit, ω is the angular frequency, and the exponent n can formally vary between 1 and 0, depending on system properties; while, normally, it varies between 1 and 0.75, when CPE is used to model the double layer response). We anticipate that this semiempirical constant phase element would also take into account the parasitic capacitance of the

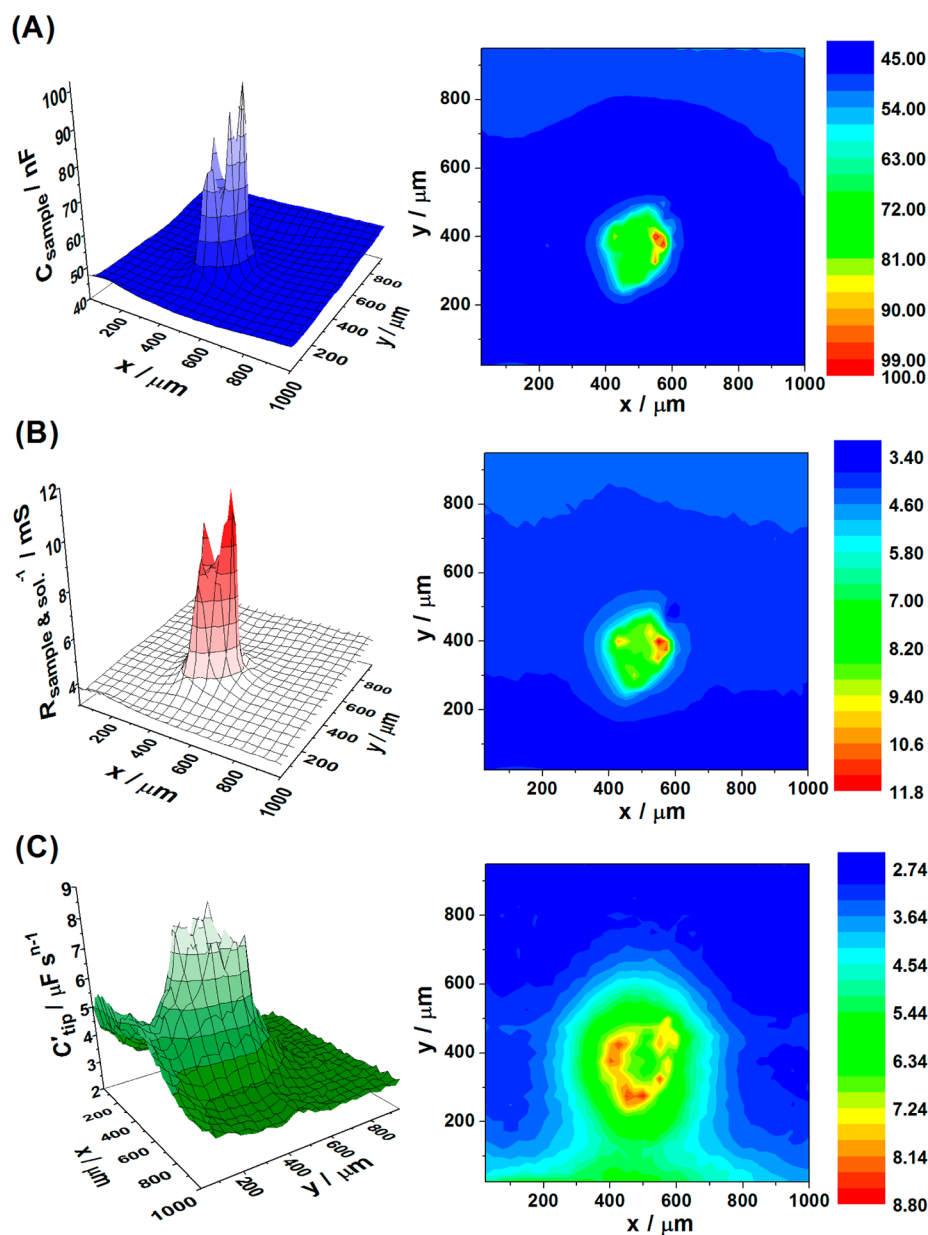


Figure 4. (A–B) spatial distributions of the key parameters describing solid/liquid interfaces: (A) the electric double layer capacitance and (B) the inverse of the charge transfer resistance (which also contains a contribution originating from the electrolyte resistance); (C) also shows the contribution of the tip which is dependent on the position of the tip and which is separated by means of the spectra fitting procedures (see text for details).

microelectrode itself as well as other capacitive effects of the tip which are difficult to predict *a priori*.

Further simplifications are related to the R'_{sample} and C'_{sample} elements which describe the response or the overall sample interface. Under relatively high frequencies used in this work and accounting for a big ratio between the overall sample surface and the specific area that is covered by the glass shield of the tip, R'_{sample} and C'_{sample} can be neglected due to relatively low contribution to the measured response. In the remaining model, it would not be possible to separate the local charge transfer resistance R_{sample} and the solution resistance R_{sol} connected in parallel. Therefore, the resultant EEC to be evaluated by the fitting procedures is shown in Figure 1B, where $R_{\text{sample \& sol}}^{-1} = R_{\text{sample}}^{-1} + R_{\text{sol}}^{-1}$ and L is an additional inductance necessary to account for the nonideal behavior of the potentiostat at higher frequencies (the apparent L -values

were found in this work to be lower than ~ 2 mH and taken into account during the automatic fitting, if necessary).

Figure 2 shows examples of dependencies of different parts of the impedance on spatial coordinates x and y at two frequencies, 270 Hz and 8 kHz. One can distinguish the area of the artificial defect in the polymer coating (approximately in the middle of the pictures of the surfaces). However, it is clear from the figure that the AC-SECM image of the surface is largely dependent on the probing frequency and on selection of the exact part of the impedance response for the imaging. While for many applications, visualization at higher frequencies would be already appropriate, a potentially much deeper insight into the localized surface and interfacial processes can be achieved if further analysis and fitting of all available impedance data to the physical model (EEC) is performed, as demonstrated below.

The local impedance spectra fit well to the simplified equivalent circuit shown in Figure 1B, both outside the artificial defect area and over the defect area (Figure 3). Some other common EECs were also checked according to procedures described elsewhere;^{25,30} however, the model shown in Figure 1B demonstrated the best accordance with all statistical criteria selected for the evaluation of models and fitting quality (see the Experimental Section and refs 25, 30, and 31 for further details).

Figure 4 summarizes the output of the 4D AC-SECM data fitting as the following corresponding functions of spatial coordinates:

- (i) the interfacial capacitance of the sample $C_{\text{sample}}(x,y)$ (Figure 4A);
- (ii) the sum of the inverses of the sample and electrolyte resistance $R_{\text{sample\&sol}}^{-1}(x,y)$ (Figure 4B);
- (iii) the contribution of the tip interface and parasitic capacitances of the microelectrode at different positions during the scan as $C'_{\text{tip}}(x,y)$ (Figure 4C).

As can be seen from Figure 4, the parameters obtained after the data fitting are different and largely depend on the position of the tip.

Figure 4A represents local variation of the interfacial capacitance of the sample as a 3D plot (left) and as a 2D map (right). The $C_{\text{sample}}(x,y)$ capacitance values obtained over the sample surface coated with the thin film fluctuate around ~45 nF, which is in accordance with the properties of the sample and the effective dimensions of the microelectrode (tip + glass shield). Approximately in the middle of the scanned area, where the ~220 μm circular defect had been introduced, the $C_{\text{sample}}(x,y)$ capacitance values increase up to 70–100 nF. This can be explained with the fact that partially exposed metallic surface can directly form a compact double layer consisting of the water molecules, anions, and cations from the electrolyte. Additionally, the thickness of the protective organic coating is significantly reduced at the defect site that increases the measured capacitance values, even if the metal surface is not directly exposed to the electrolyte. It should be noted here that the contrast of the $C_{\text{sample}}(x,y)$ picture is high and corresponds to the AC-SECM pictures taken at higher frequencies (Figure 2D–F). The pinhole dimensions (~220 μm in diameter) are also in correspondence with the real geometrical size of this defect. However, we anticipate that the $C_{\text{sample}}(x,y)$ provides visualization using a parameter (interfacial or the double layer capacitance) which has a more clear physical meaning and is intuitively understandable for experts working in various fields of science and technology, compared to just different impedance values taken at different frequencies and plotted as a function of spatial coordinates as used in other LEIS approaches.

The inverse of the resistance which contains contributions originating from the electrolyte resistance and the charge transfer, $R_{\text{sample\&sol}}^{-1}(x,y)$, is shown in Figure 4B. The resistance outside the area over the pinhole mainly originates from the resistance of the electrolyte, R_{sol} . The latter monotonously varies with the tip position relative to the reference electrode with the average value of ~250 Ohm, in good agreement with an expected resistance of the 1 mM KClO_4 electrolyte. In the area over the circular defect, the $R_{\text{sample\&sol}}^{-1}(x,y)$ increases drastically revealing electrochemical processes which originate from the exposed metallic surface. The electrolyte-exposed metal surface becomes electroactive under the *ac*-perturbation due to corrosion, reactions with dissolved oxygen, specific

adsorption/desorption, etc. While many features of the $R_{\text{sample\&sol}}^{-1}(x,y)$ picture over the area of the defect are different compared to the corresponding features in Figure 4A, the overall contrast is high with approximately the same size of the visualized circular defect (~220 μm in diameter). Having corrected Figure 4B by the contribution from the R_{sol} resistance over the area of the pinhole, it provides valuable information about the charge transfer resistance R_{ct} of the local electrochemical processes

$$R_{\text{sample\&sol}}^{-1}(\text{corrected}) \approx R_{\text{ct}}^{-1} \approx (\partial i_{\text{Faradaic}} / \partial E)$$

where i_{Faradaic} is the local current due to a Faradaic reaction (e.g., electrocatalytic reaction or corrosion), and E is the electrode (sample) potential. This opportunity converts the 4D AC-SECM into one of only a few techniques capable of quantifying the local kinetics of electrocatalytic reactions, corrosion, metal dissolution, or other important processes with high spatial resolution.

Finally, Figure 4C shows the contribution of the capacitive effects of the tip which is also dependent on the position of the tip due to different reasons, such as the following: various contributions from metal cations released by the sample at the pinhole site to the electrolyte, possible random contaminations, different parasitic capacitances, etc. The values $C'_{\text{tip}}(x,y)$ are much higher (several microfarads) than the sample/electrolyte interface capacitance values $C_{\text{sample}}(x,y)$, as expected, taking into account parasitic capacitances of the microelectrode itself. It should be noted here that the CPE-exponent values were found to change with the position of the tip. On average, the CPE-exponent values were ~0.8; however, we would not speculate here about a possible origin of this nonideal behavior (it is outside the scope of this work), as the tip/electrolyte interface represents a less defined system compared to the Pt(111) single crystal, where we observe low CPE-exponent values at the electrode potentials at which structural effects in the Pt(111)/electrolyte interface occur.³²

Having compared Figure 4C and Figure 2A–C, it is possible to conclude that a lower spatial resolution of the classical AC-SECM pictures at lower perturbing *ac*-frequencies (Figure 2A–C) is largely due to the contribution of the tip (as well as the microelectrode itself) response. The ability to distinguish contributions from the probe and the sample itself provide additional unique opportunities in many applications, as the tip can also play an “active” role to generate reactants and consume products in different modes of electrochemical microscopies.

CONCLUSIONS

In summary, we have demonstrated for the first time that the ability to record localized impedance spectra being combined with modern achievements in the field of chemometrics to fit large EIS-data sets to the physical models of the interface show promise to bring AC-SECM to a much higher level of informative power of the technique. Experiments using the model sample show that the impedance analysis of the 4D AC-SECM data in terms of EECs efficiently decomposes the overall *ac*-response into constituents related to the microelectrode, the interfacial capacitance of the sample, and the localized Faradaic processes at the sample surface. This eliminates many common methodological problems of the LEIS related to the frequency dependence of the actual pictures of the surface and difficulties with data interpretation. The proposed approach allows visualization of spatial distributions of the key parameters

describing solid/liquid interfaces enabling easier interpretation of the AC-SECM data, as these parameters have clearer physical meaning and are intuitively understandable for experts working in various fields of science and technology. Thus the modified AC-SECM approach can offer a unique insight into the localized processes at the interface which is not possible to achieve using classical LEIS-techniques.

AUTHOR INFORMATION

Corresponding Author

*Phone: +49(0)234 32 29433. E-mail: aliaksandr.bandarenka@rub.de (A.S.B.). Phone: +49 (0) 234 3226200. E-mail: wolfgang.schuhmann@rub.de (W.S.).

Notes

The authors declare no competing financial interest.

ACKNOWLEDGMENTS

Financial support by the EU and the state NRW in the framework of the High Tech. The NRW program is gratefully acknowledged. The authors additionally acknowledge financial support in the framework of Helmholtz-Energie-Allianz "Stationäre elektrochemische Speicher und Wandler" (HA-E-0002) and the Cluster of Excellence RESOLV (DFG EXC-1069).

REFERENCES

- (1) Kolb, D. M. *Angew. Chem., Int. Ed.* **2001**, *40*, 1162.
- (2) Conway, B. E. *J. Electroanal. Chem.* **2002**, *524–525*, 4.
- (3) Tian, Z.-Q.; Ren, B. *Annu. Rev. Phys. Chem.* **2004**, *55*, 197.
- (4) Hugelmann, M.; Hugelmann, P.; Lorenz, W. J.; Schindler, W. *Surf. Sci.* **2005**, *597*, 156.
- (5) Garcia-Araez, N.; Rodriguez, P.; Navarro, V.; Bakker, H. J.; Koper, M. T. M. *J. Phys. Chem. C* **2011**, *115*, 21249.
- (6) Koper, M. T. M. In *Catalysis in Electrochemistry: From Fundamentals to Strategies for Fuel Cell Development*; Wiley-VCH: New York, 2011; pp 223–247.
- (7) Inzelt, G. *Electrochemical Quartz Crystal Nanobalance in Electroanalytical Methods*, 2nd ed.; Scholz, F., Ed.; Springer: 2010; Part II.10.
- (8) Bondarenko, A. S.; Stephens, I. E. L.; Hansen, H. A.; Perez-Alonso, F. J.; Tripkovic, V.; Johansson, T. P.; Rossmeyl, J.; Nørskov, J. K.; Chorkendorff, I. *Langmuir* **2011**, *27* (5), 2058.
- (9) Eckhard, K.; Schuhmann, W. *Analyst* **2008**, *133*, 1486.
- (10) Eckhard, K.; Erichsen, T.; Stratmann, M.; Schuhmann, W. *Chem.—Eur. J.* **2008**, *14*, 3968.
- (11) Magnussen, O. In *Electrochemistry at the Nanoscale*; Schmuki, P., Virtanen, S., Eds.; Springer Science+Business Media: New York, 2009.
- (12) Bard, A. J.; Faulkner, L. R. *Electrochemical methods. Fundamentals and Applications*, 2nd ed.; Wiley: 2001.
- (13) Isaacs, H. S.; Kendig, M. W. *Corrosion* **1980**, *36*, 269.
- (14) Lillard, R. S.; Moran, P. J.; Isaacs, H. S. *J. Electrochem. Soc.* **1992**, *139*, 1007.
- (15) Zhou, F.; Thierry, D.; Isaacs, H. S. *J. Electrochem. Soc.* **1997**, *144*, 1957.
- (16) Katemann, B. B.; Schulte, A.; Calvo, E. J.; Koudelka-Hep, M.; Schuhmann, W. *Electrochem. Commun.* **2002**, *4*, 134.
- (17) Huang, V. M.; Wu, S.-L.; Orazem, M. E.; Pèbère, N.; Tribollet, B.; Vivier, V. *Electrochim. Acta* **2011**, *56*, 8048.
- (18) Eckhard, K.; Shin, H.; Mizaikoff, B.; Schuhmann, W.; Kranz, C. *Electrochem. Commun.* **2007**, *9*, 1311.
- (19) Diakowski, P. M.; Ding, Z. *Phys. Chem. Chem. Phys.* **2007**, *9*, 5966.
- (20) Schulte, A.; Belger, S.; Etienne, M.; Schuhmann, W. *Mater. Sci. Eng., A* **2004**, *378*, 523.
- (21) Gebala, M.; Schuhmann, W.; La Mantia, F. *Electrochem. Commun.* **2011**, *13*, 689.
- (22) Bondarenko, A. S. *Anal. Chim. Acta* **2012**, *743*, 41.
- (23) Bondarenko, A. S.; Ragoisha, G. A. In *Progress in Chemometrics Research*; Pomerantsev, A. L., Ed.; 2005; pp 89–102.
- (24) Ragoisha, G. A.; Bondarenko, A. S. *Solid State Phenomena* **2003**, *90–91*, 103.
- (25) Berkes, B. B.; Maljusch, A.; Schuhmann, W.; Bondarenko, A. S. *J. Phys. Chem. C* **2011**, *115*, 9122.
- (26) Pomerantsev, A. L. *Chemom. Intell. Lab. Syst.* **2003**, *66*, 127.
- (27) Pajkossy, T. *J. Electroanal. Chem.* **1994**, *364*, 111.
- (28) Pajkossy, T.; Kolb, D. M. *Electrochim. Acta* **2008**, *53*, 7403.
- (29) Motheo, A. J.; Sadkowski, A.; Neves, R. S. *J. Electroanal. Chem.* **1997**, *430*, 253.
- (30) Berkes, B. B.; Inzelt, G.; Schuhmann, W.; Bondarenko, A. S. *J. Phys. Chem. C* **2012**, *116*, 10995.
- (31) Ragoisha, G. A.; Bondarenko, A. S. *Electrochim. Acta* **2005**, *50*, 1553.
- (32) Tymoczko, J.; Schuhmann, W.; Bandarenka, A. S. *Electrochem. Commun.* **2013**, *27*, 42.